Check for updates

Effect of low dissolved oxygen concentration on the defects and composition of regenerated passive film of Ti-6Al-4V alloy under continuous wear

Xinyu Du,[ab] Wei Shi 🆔 *[ab] and Song Xiang 🆔 [ab]

Tribocorrosion is one of the most common forms of failure of biomedical titanium alloys. As the passive film of titanium alloys is highly dependent on oxygen conditions, the passivation behavior and the microstructure of the passive film of Ti-6Al-4V under tribocorrosion in 1 M HCl with a low dissolved oxygen concentration (DOC) were studied by means of electron probe microanalysis (EPMA), Ar-ion etched X-ray photoelectron spectroscopy (XPS), focused ion beam (FIB) milling and high resolution transmission electron microscopy (HRTEM). The results showed that the protective ability of the regenerated passive film decreased sharply under low DOC. Al and V ions dissolved in excess, and a large number of oxygen atoms entered the matrix, leading to internal oxidation. Structural characterization indicated that Ti atoms occupied more metal lattice points in the regenerated passive film and that the high dislocation density in the deformed layer caused by wear facilitated the diffusion of Al and V. Finally, the first-principles calculation showed that Al had the minimum vacancy formation energy.

Introduction

Ti-6Al-4V has a high specific strength, excellent mechanical properties, is anti-corrosive, is a highly biocompatible alloy[1–4] and is often considered as an ideal implant material. However, early service failure always occurs with titanium implants especially when functioning as active components, such as in human joints.[5] The results of certain studies indicated that the tribocorrosion accelerated the damage to titanium implants.[5,6] The anticorrosion mechanism of Ti highly relies on the passive film of the implant surface. Hanawa *et al.*[7] found that the concentration of Cl ions in serum and tissue fluid is 113 and 117 mEq L^{-1}, respectively, and the dissolved oxygen concentration in body fluid is 1/4 of that in air. Lower dissolved oxygen concentrations (DOCs) in tissue liquid inhibit the generation of passive film, which results in weaker protectivity.[8–10]

In the tribocorrosion process, the passive film of the joint undergoes a break/repair process.[11] The repair speed of the passive film is determined by the corrosion rate of tribocorrosion. During the tribocorrosion process, if there is no oxygen, the repair is delayed. During this delay, it is very likely that the sample is in a state without passive film protection, leading to the problem of the accelerated dissolution of harmful elements. In fact, many

active joints were observed to have damage of the implant surface and necrosis of the surrounding tissues.[12,13] A high level of Al and V ions was extracted from the tissue fluid near a joint, which showed that the tribocorrosion reaction occurred.[14] These metal ions may hinder the process of bone integration, leading to implant loosening.[15–17] In addition, some metal chips produced by abrasion may cause adverse effects, such as cell damage, inflammation, allergic reactions, and rash.[18–20] The passive film of titanium alloys can be effectively regenerated to achieve a passivation state after the surface is mechanically damaged.[21,22] As a result, rapid passivation can prevent the corrosion dissolution of and release of Al and V elements from titanium alloys. However, just the opposite actually occurs: the surface of Ti implants are severely corroded before the design.[23] Therefore, it is reasonable to consider whether the passivation process near the joint is slowed down due to the relatively insufficient dissolved oxygen in the tissue fluid. Long recovery times will lead to the release of the passive films of Al and V. Thus, wear under low DOC and the difference in the structure and performance of regenerated passive films should be considered.

Xin Lu[24] *et al.* studied the change in wear resistance and corrosion resistance of the alloys with different Cu contents. M. K. Diamah *et al.*[25] found that different alloys (Ti-Grade 2, Ti6Al4V and Ti6Al4V-ELI) showed different wear and corrosion properties in phosphate buffer solution (PBS) and phosphate buffer solution with bovine serum albumin (PBS + BSA). Most previous studies focused on the effects of different loads, wear frequencies, and element compositions on the tribocorrosion properties of titanium alloys. Few studies have concentrated on the effect of dissolved oxygen on the passivation process of Ti-

[a]Guizhou Key Laboratory of Materials Mechanical Behavior and Microstructure, College of Materials and Metallurgy, Guizhou University, Guiyang 550025, P. R. China. E-mail: wshi@gzu.edu.cn

[b]National & Local Joint Engineering Laboratory for High-Performance Metal Structure Material and Advanced Manufacturing Technology, Guizhou University, Guiyang 550025, China

6Al-4V during tribocorrosion. Li *et al.*[26] found that the removal of DO inhibit the conversion of TiO₂, which hindered the passivation of titanium alloys and increased the passivation current density. However, when titanium alloys are worn under low DOC, it is still a question whether the resulting regenerated passive film can protect the substrate well afterward.

In conclusion, although some effects of dissolved oxygen have been studied, there are still few studies on the performance of regenerated passive films under different DOCs during wear. In order to explore the effects of different DOCs on the properties of regenerated passivation films were studied by inductively coupled plasma-atomic emission spectroscopy (ICP-OES) was used to quantify the number of ions released during wear. Subsequently, the structure and composition information of the regenerated passive film and its interior were obtained by electron probe microanalysis (EPMA), X-ray photoelectron spectroscopy (XPS), and high-resolution transmission electron microscopy (HRTEM). The first-principles calculation verified the preferential tendency of metal ions leaving the matrix to form vacancies in the alloy.

Experimental methods

Sample preparation

The experimental material was a Ti-6Al-4V round bar in the forged state. The chemical composition of the Ti-6Al-4V alloy is shown in Table 1. A Φ 16 mm × 10 mm cylindrical sample was cut from the round bar with the wire cutter and sealed in 20 mm diameter epoxy resin. Then, the sample was ground from 80# to 2000#. Then, the sample was polished with Cr₂O₃ polishing solution until there was no noticeable scratch on the surface. Finally, the sample was ultrasonically cleaned with ethanol for later use.

Installation

In this study, we designed a reciprocating wear device, as shown in Fig. 1. The dissolved oxygen in the solution was removed by 1 h bubbled high purity nitrogen, which was confirmed by repeated measurements with a dissolved oxygen tester (JPBJ-610L, REX, China). When no gas was bubbled into the solution, the dissolved oxygen concentration measured was 1.51 ppm. After 1 h N₂ was bubbled, the dissolved oxygen concentration measured was 0.03 ppm, and the dissolved oxygen concentration measured was 4.76 ppm after 1 h air was bubbled. In the device, ZrO₂ ceramic ball was used as a pair of wearing parts. Then, an electric stirrer was inserted into the electrolytic cell to stir the solution in the experiment. In addition, for the reciprocating wear of 10 mm stroke, a load of 10 N was applied. The wear speed was 14 mm s⁻¹, and the wear time was 30 min. To ensure the reproducibility of the experiment, three parallel experiments were carried out.

Electrochemical testing

All experiments were conducted in 1 M HCl solution at 28 °C. A titanium alloy sample was used as the working electrode (WE), a saturated calomel electrode was used as the reference
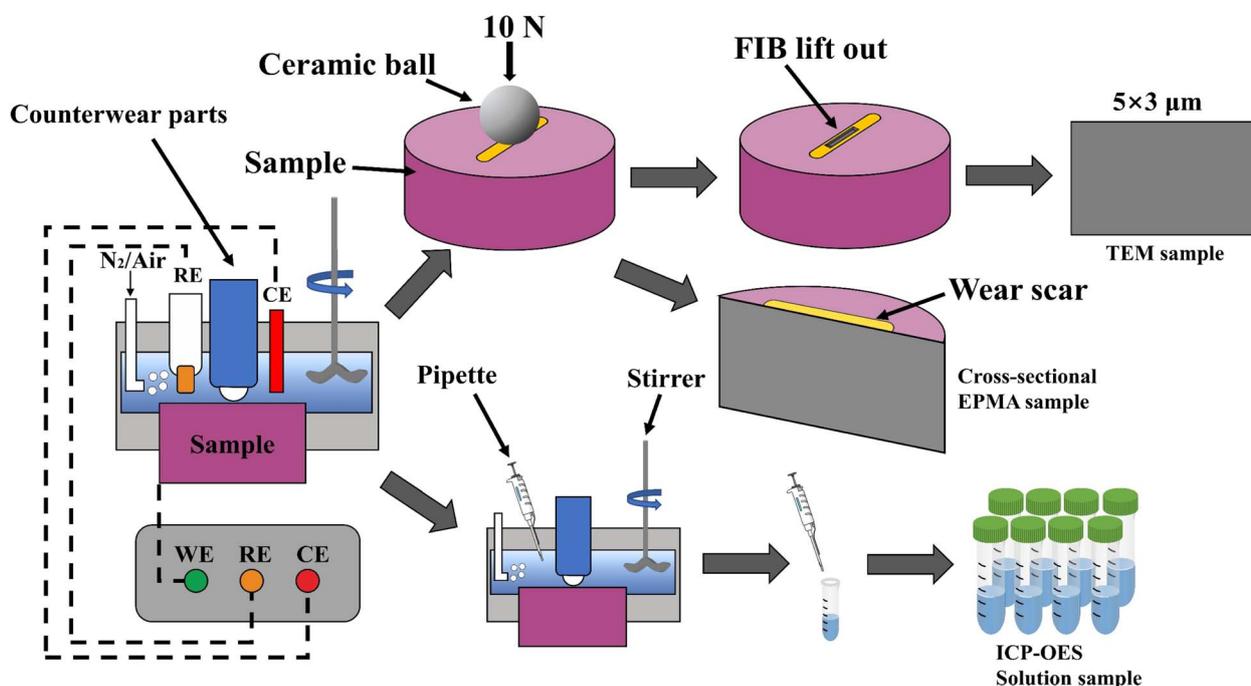
Table 1 Chemical composition of Ti-6Al-4V alloy (wt%)

Ti	Al	V	Fe	Si	C	N	O	H
Bal.	6.32	4.13	0.17	<0.01	0.007	0.003	0.11	0.0009

Fig. 1 Schematic diagram of experimental method.

electrode (RE), and a 40 mm × 10 mm platinum plate was used as the counter electrode (CE). Before the potentiodynamic polarization curve test, the open circuit potential test (OCP) was conducted for 30 min to stabilize the passive film on the working electrode surface. Electrochemical information was collected at a scanning rate of 0.5 mV s^{-1} within the voltage range of -0.3 V$_{\text{SCE}}$ to 2 V$_{\text{SCE}}$. Before the potentiostat polarization curve test, cathodic polarization was performed for 5 min at -1.2 V$_{\text{OCP}}$ potential. In this way, the passive film formed on the surface of the titanium alloy in air was eliminated. Then, 60 min of anodic polarization was conducted at 0.5 V$_{\text{OCP}}$ potential. In this way, a new passive film was formed on the titanium alloy in the solution, making it stable. Then, tribocorrosion was carried out for 30 min at a 0.5 V$_{\text{OCP}}$ anode potential to collect electrochemical information under tribocorrosion conditions.

Morphological characterization

After the wear experiment, the samples were photographed with an OLS5000 laser confocal microscope (Olympus Corporation, Japan) to analyze the 3D topography and profile of the wear scar, and the wear scar morphology under different DOCs was observed.

ICP-OES analysis

An American Thermophile iCAP 7200 Inductively Coupled Plasma Emission Spectrometer (ICP-OES) was used. Twelve samples were collected with a 5 ml pipette gun every 10 min to detect the concentrations of Ti, Al and V. Considering that the total volume of the solution was 150 ml before the start of the experiment, the volume of the solution gradually decreased with increasing sampling time. With the release of elements, the concentration of the elements in the solution was concentrated. Thus, we corrected the detected concentration, and the correction formula was:

$$C_{\text{P}} = C_0 \times V_{\text{P}}/V_0 \qquad (1)$$

where C_{P} is the concentration after correction, C_0 is the test concentration before correction, V_{P} is the volume of solution left in the electrolytic cell during sampling, and V_0 is the total volume of solution before the experiment.

EPMA tests

The sample was cut along the wear scar by wire cutting, and the cut sample was polished. The section of the wear scar was tested by EPMA on JXA-8530F PLUS test equipment to determine the elementary composition distribution of the wear scar section.

TEM measurements

The cross-section sample of the film was prepared by a double-beam focused ion beam (FEI LD Helios G5UX). The platinum layer was deposited before FIB grinding to protect the passive film. Transmission electron microscopy (TEM, FEI Talos F200X) was utilized to observe the microstructure of the alloy at 200 kV voltage.

XPS analysis

The chemical state of the wear scar surface and subsurface of samples with different etching depths (0 nm, 2.5 nm, 5 nm, 10 nm, 20 nm) was analyzed by X-ray photoelectron spectroscopy (XPS) using a Thermo Scientific K-Alpha. Sputtering was performed by Ar ion etching at an approximate rate of 0.18 nm s^{-1}. The C 1s = 284.8 eV binding energy was used as the energy standard for charge correction to obtain the most appropriate chemical significance information.

Calculation methods

The vacancy formation energy between the α and β phases was calculated using Vienna *ab initio* simulation package VASP software, and the priority order of dissolution was determined by the vacancy formation energy. The calculations are based on density functional theory and the projector augmented wave (PAW) formalism, which is implemented with the Vienna *ab initio* simulation package (VASP) code.[27] For the exchange–correlation function, the Perdew–Burke–Ernzerhof (PBE) functional with the generalized gradient approximation (GGA) is utilized. The slab model of a 5 × 5 × 1 supercell with a 20 Å vacuum layer along the *z*-axis is constructed to analyze the metal elements dissolution processes on the (001) and (110) surfaces. According to the conventional strategy, we fixed the bottom layer of the slab model to represent the bulk environment and relaxed the top layer to reflect the true situation of surface atoms. An energy cutoff of 500 eV for plane wave expansion, along with a suitable Monkhorst–Pack *k*-point setting of 2 × 2 × 1, is adequate to ensure that the total energy and force converge at 10^{-5} eV and 0.01 eV Å^{-1}.

The vacancy formation energy was calculated by removing an atom from a complete matrix to generate the energy required to create a vacancy. The α/β phase model was built based on ref. [28], as shown in Fig. 2. To compare the difficulty of different atoms breaking away from the matrix, the vacancy formation energies of six cases were introduced. The vacancy formation energy of different atoms was expressed as:[29]

$$E_{\text{X}}^{\text{V}} = E_{\text{X}} - E_0 + \mu_{\text{X}} \qquad (2)$$

where E_{X}^{V} is the energy required for the X atom to leave the matrix, E_{X} is the energy after one X atom is removed to generate vacancies, E_0 is the energy of a complete matrix consisting of 50
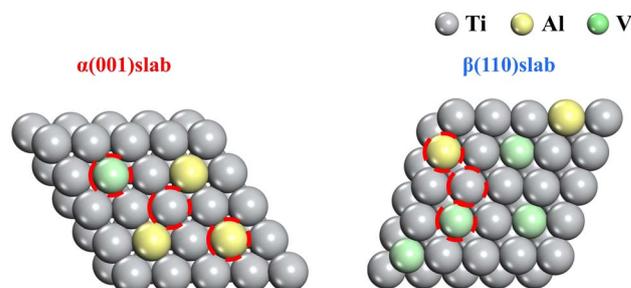

Fig. 2 Schematic diagram of atomic location for the vacancy formation energy calculation.

atoms without vacancies, and μ_X is the energy of a single X atom.

Experimental results

Electrochemical test

The potentiodynamic polarization curve is shown in Fig. 3. The corrosion potential of the sample under low DOC negatively shifted. This phenomenon clearly showed that the passivation efficiency of Ti-6Al-4V highly depended on the DOC in solution, which caused serious corrosion under low DOC. Additional evidence was observed at the potential near -0.55 V_{SCE}, and the typical current peak at this potential proved that a transition occurred from activation to passivation. However, the anodic branch of the polarization curve does not exhibit a linear correlation between E and $\log I$, rendering it unsuitable for Tafel fitting. Therefore, we have relied on data from the cathodic branch (range from -70 mV to -120 mV $vs.$ OCP) to calculate i_{corr}, as shown in Table 2. Apparently, the increase in corrosion current was mainly attributed to the lower DOC inhibiting the formation of the passive film and keeping the passive film in a soluble state. Finally, the passivation current under low DOC was significantly higher than that under high DOC, which indicated that the passive film formed under low DOC had a higher defect density and weaker corrosion resistance.

Moreover, there was no difference in the cathodic reaction part with a change in DOC, which indicated that the hydrogen evolution reaction (HER)[9] dominated the cathodic process in an acidic environment. In addition, an anode peak at 1.5 V_{SCE} was found in the curves, which was reported in ref. 30 and 31. The changes in the structure and composition of the passive film led to the appearance of the anode peak, and the nonstoichiometric titanium oxides near this potential were converted into TiO_2. However, the transition process to TiO_2-dominated titanium oxide was inhibited in the solution with low DOC, resulting in a smaller anode peak. Under high DOC, more TiO_2 is formed on the alloy surface, which also leads to the worse protection performance of the passive film under low DOC compared to that under high DOC.

According to literature,[32,33] in addition to reacting with dissolved oxygen, Ti can also react with H_2O to form a passive film. In this reaction, Ti^{4+} reacts with H_2O to form $(Ti(OH)_2)^{2+}$. After dehydration and crystallization, a stable TiO_2 passive film is established. A passivation zone was still observed under the condition of low dissolved oxygen. This showed that the titanium alloy can form a passive film with H_2O after dissolved oxygen removal. However, passive films formed by H_2O are still soluble at a certain potential. Even if this type of passive film forms, its protection performance is still inferior to that of the passive films formed by a high DOC, and its defect concentration is higher, so it is a metal-excess semiconductor.[26]

Tribocorrosion test

The potentiostatic anodic polarization curve under tribocorrosion with different DOCs in 1 M HCl solution is shown in Fig. 4. It was observed that the change in dissolved oxygen had little effect on the wear performance of titanium alloy, but the current under high DOC was slightly smaller. This may be due to the higher efficiency of passive film repair, which to some extent inhibits corrosion during wear. As the passive film was removed from the surface, the titanium alloy under different DOCs was directly exposed to the solution, which resulted in the anodic dissolution current of titanium alloy at this potential being hundreds of times higher than that under the passivation state.

According to Faraday's law,[16,34] it was calculated that the corrosion loss under high DOC and low DOC was 4.20×10^{-5} g and 4.42×10^{-5} g, respectively. The corrosion loss of the sample
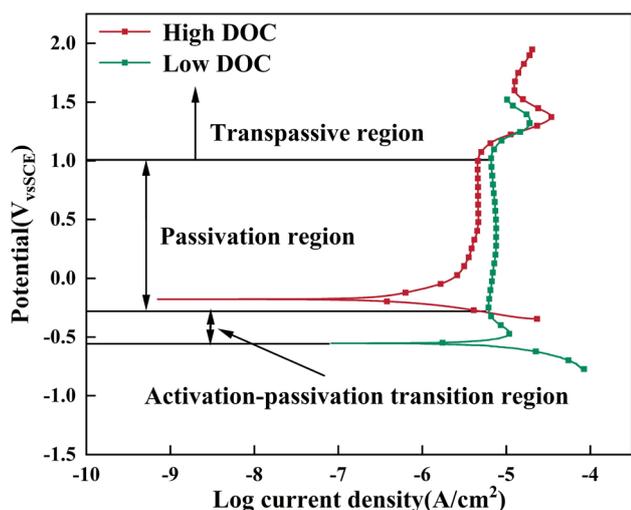
Table 2 Electrochemical parameters of different DOCs

	E_{corr} (V)	i_{corr} (A cm^{-2})	$-\beta_c$ (mV)	Corrosion rate (mm A^{-1})
High DOC	-0.178	6.301×10^{-7}	114.79	0.006
Low DOC	-0.554	9.076×10^{-6}	172.71	0.080

Fig. 3 Potentiodynamic polarization curve of Ti-6Al-4V alloy under high DOC and low DOC in 1 M HCl solution.
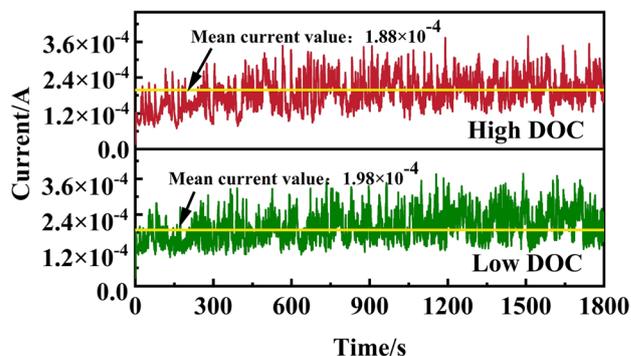

Fig. 4 Potentiostatic anodic polarization curve of Ti-6Al-4V alloy under high DOC and low DOC in 1 M HCl solution.
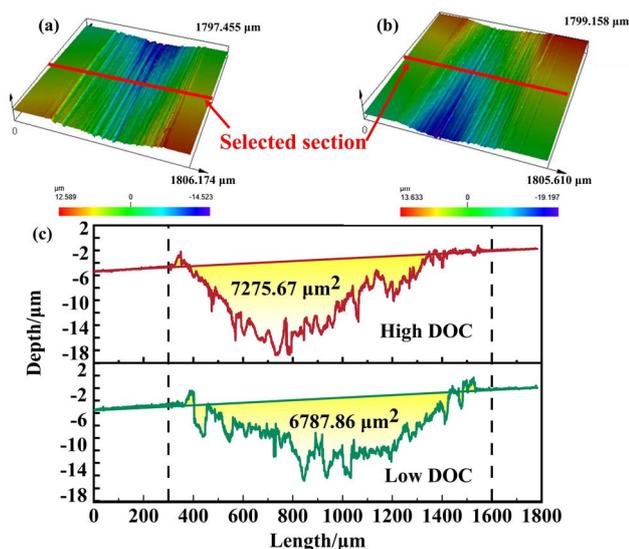
Fig. 5 3D morphology of wear scar under different DOC: (a) high DOC, (b) low DOC, (c) the profile of the wear.

under low DOC was greater in the tribocorrosion process. The low DOC inhibited the formation of a passive film on the surface of the titanium alloy, and the damaged passive film was not repaired in time, which directly exposed the metal matrix directly exposed to the acid solution, thus worsening the tribocorrosion performance under low DOC.

Laser confocal scanning was used to observe the internal 3D shape of the wear scar and compare the differences in the profile. The reproducibility of the experiment was ensured by selecting the contour surface 3 times. It can be observed from Fig. 5a and b that the inside of the wear scar was full of parallel grooves, which indicated that a large number of third bodies (other particles except for the wear parts and objects to be worn) acted as abrasives. The results showed that abrasive wear acted on the surface of the titanium alloy as one of the wear mechanisms. However, during wear, some metal elements broke away from the matrix and diffused into the solution. These free metal elements combined with free oxygen in solution to form oxide particles to deposit on the surface, which participated in the

wear as a third body (other particles except for the worn parts and objects to be worn).

Generally, the method for evaluating the total volume loss in the tribocorrosion of samples was:[35]

$$V_{\text{total}} = V_{\text{chemical}} + V_{\text{mechanical}} \tag{3}$$

where V_{total} is the total loss; V_{chemical} is the amount of electrochemical corrosion loss, and $V_{\text{mechnical}}$ is the mechanical wear loss.

During the potentiostatic test, it was calculated that the V_{chemical} under low DOC was greater. However, the profile area obtained by laser confocal scanning was decreased under high DOC. This indicated that the $V_{\text{mechanical}}$ was greater under high DOC. Under high DOC, more dissolved oxygen formed more oxide particles, which led to a larger $V_{\text{mechanical}}$ under high DOC.

Dissolution measure

ICP-OES was used to monitor the change of ion concentration in solution during tribocorrosion. Fig. 6a shows that almost no dissolved Ti ions were detected in the 2nd sampling (immersed for 20 min). This performance showed good protection of the passive film without wearing. Unfortunately, when wearing started, the ion concentration intensively increased, regardless of the presence of Ti, Al or V ions. After the 5th sampling, the wearing stopped, the concentration accumulation was due to the subsequent corrosion during the passivation recovery, and the increasing rate of the concentration reflected the corrosion rate of ions. As shown in Fig. 6a, Ti ions remained in a state of continuous dissolution, but obviously, the dissolution rate decreased after the wear stopped. This phenomenon showed that the protective performance of the titanium alloy passive film could not be recovered in a short time after mechanical damage. The elements in the alloy still maintained a high dissolution rate for a period of time under an acidic environment after wear stopped, which caused harmful metal ions to enter the human body fluid circulation. Interestingly, the dissolution rate of Ti ions under low DOC seemed to be slightly lower than that under high DOC. This was due to the cathodic protection effect of the accelerated dissolution of Al and V ions under low DOC, which hindered the dissolution of Ti particles.
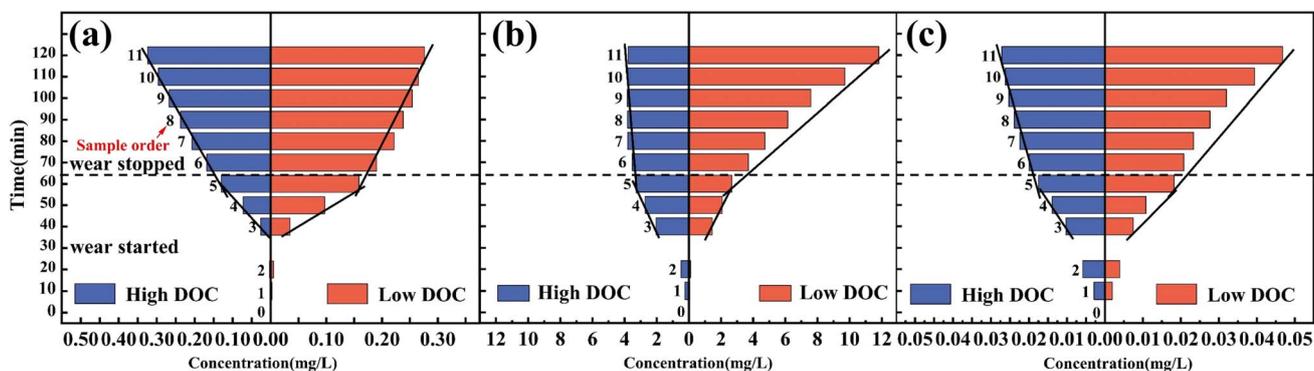

Fig. 6 ICP-OES analysis of element concentrations in 1 M HCl solution over time: (a) Ti, (b) Al, (c) V.

As shown in Fig. 6b, the dissolution of Al under high DOC immediately stopped after the wear stopped, which indicated that a fast generation of oxide film inhibited corrosion. Under low DOC, the dissolution rate significantly increased, suggesting that active corrosion occurred without the protection of the passive film. In addition, similar dissolution trends were also
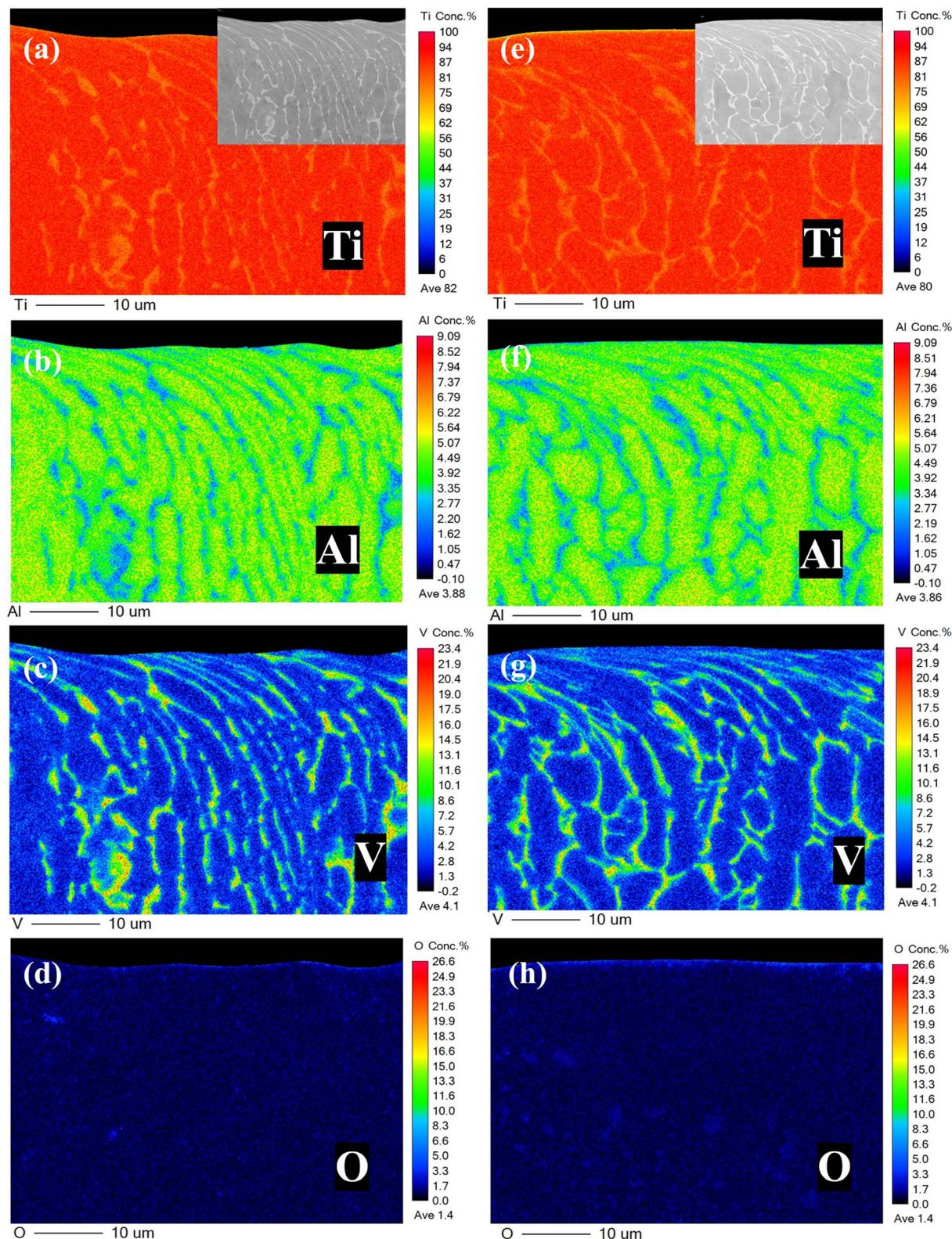

Fig. 7 Wear scar section under different DOCs: (a–d) element distributions of Ti, Al, V, O in the wear scar section under high DOC, (e–h) element distributions of Ti, Al, V, O in the wear scar section under low DOC.
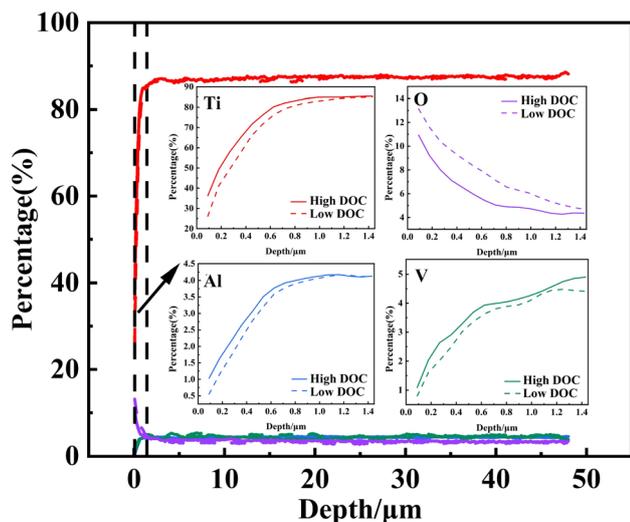
Fig. 8 Statistical chart of the EPMA element distribution map after numerical treatment.

found in the results of V (Fig. 6c). The amount of Al and V dissolved under low DOC was much greater than that under high DOC, at 312% and 174% (compare the 11th sampling). This phenomenon showed that the passive film of titanium alloy could not be immediately repaired once the passive film was damaged under the action of mechanical wear under low

DOC. During this period, the dissolution rate of harmful elements Al and V was several times higher than that under high DOC. This also confirmed our original hypothesis that the amount of dissolved Al and V far exceeded the safety limits in the body under low DOC. Moreover, from the concentration analysis, it was concluded that the regenerated passive film formed under low DOC had worse protectivity. In addition, the daily safe intake of Al is 0–0.6 mg kg^{-1}, while the daily intake of V is limited to 40 μg. Therefore, the conclusion from the ICP-OES test results is that if Ti-6Al-4V is incorporated into the human body as an implant, it impacts human health.

Section analysis

EPMA can be used to analyze the concentration distribution of a cross section with high accuracy. It can be seen from Fig. 7 that the titanium alloy surface was severely deformed within 5 μm of the surface under the effect of wear. In addition, the α phase (enriched with Al elements) and β phase (enriched with V elements)[36] became fused, blurring the interface of the α/β phases in the deformed layer. Therefore, it was difficult to observe that Ti, Al, and V had significant selective dissolution over a certain depth range (μm range). However, it was also observed that the concentration of O significantly increased at approximately 1 μm under low DOC. This phenomenon indicated that more obvious internal oxidation occurred on the surface of the titanium alloy under low DOC. It was reasonable
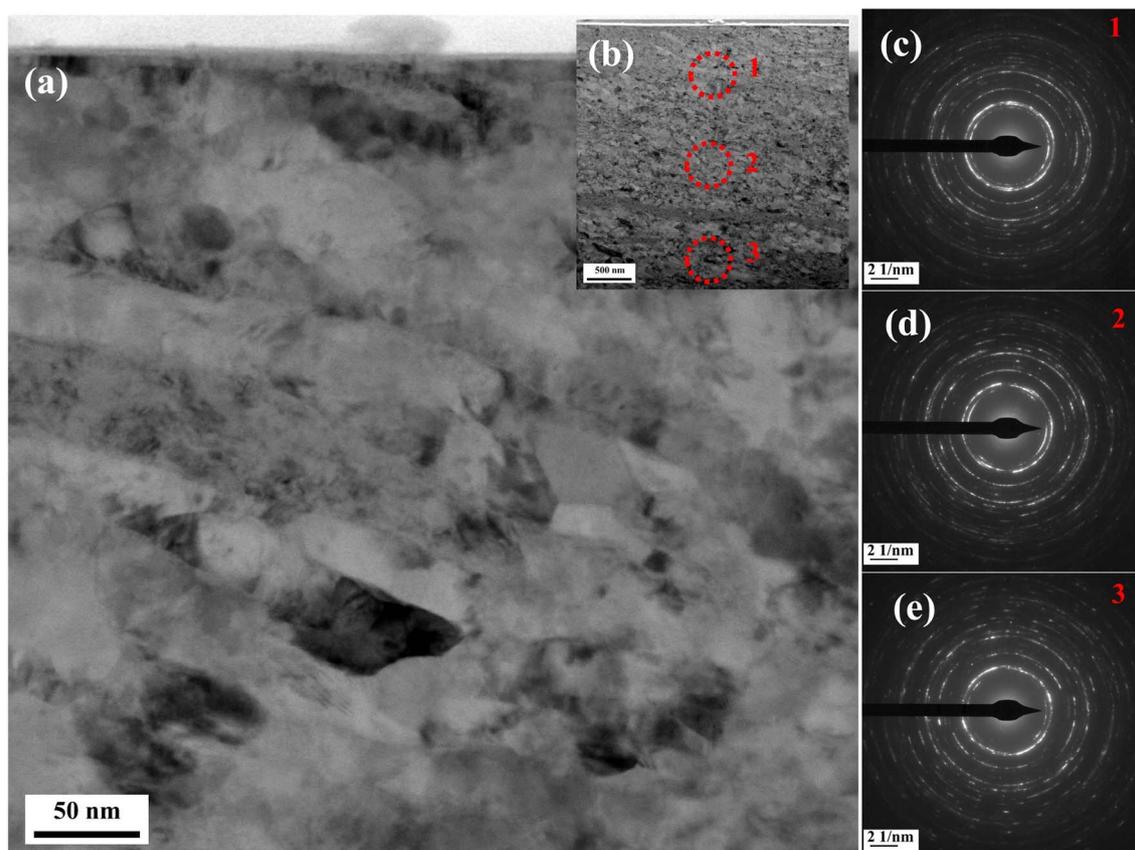

Fig. 9 Cross section of the wear scar: (a and b) cross section morphology, (c–e) diffraction spot.

to assume that there were excessive defects on the sample surface after wear.

To accurately show the gradient changes of each element at different depths, we counted the element concentrations at different depths to obtain the results shown in Fig. 8. It was observed that under high DOC and low DOC, each element in the sample had obvious differences at different depths. The Ti, Al, and V concentrations showed a certain gradient change, and the O concentration also changed from high to low, which indicated that internal oxidation did occur. From the perspective of metal dissolution, metal breaking away from the lattice caused by a lack of dissolved oxygen was more significant under low DOC. It was precisely because of the increase in metal dissolution that the internal oxidation degree in the surface layer formed under low DOC was observed at greater depths.

As shown in Fig. 8, the scanning range of the sample was 48 μm. Among the sample elements, Ti was the main element. Each element had an obvious gradient distribution within 1.4 μm, and the gradient of metal concentration under low DOC was more obvious. This showed that there was a certain degree of element diffusion in the matrix after wear. This was due to the short-circuit diffusion of elements caused by the increase in dislocation density caused by deformation, thus accelerating the diffusion of internal elements.

From Fig. 9a, it can be observed that the grain orientation of the section was inconsistent, and a large number of grains were stretched and broken due to wear deformation. Fig. 9c–e shows the diffraction spots at 1 μm, 2 μm and 3 μm from the surface, as marked in Fig. 9b. These spots showed a typical polycrystalline diffraction ring.[37] According to the diffraction
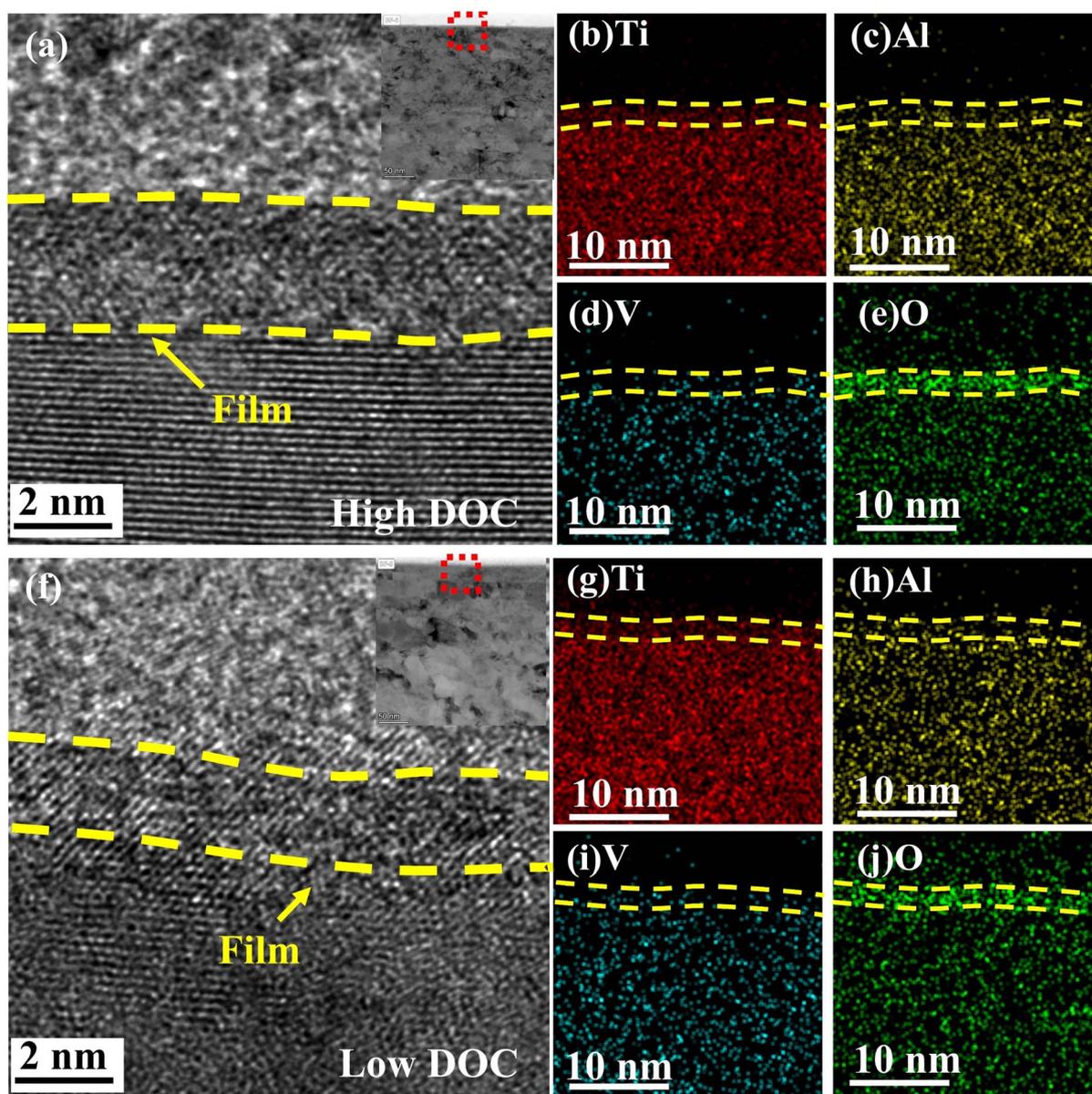

Fig. 10 Element analysis of the wear scar section: (a–e) high DOC, (f–j) low DOC.

principle of the transmission electron microscope, better continuity of the ring at different diameters means more crystals participated in diffraction. Fig. 9c shows the best continuity, indicating that the position close to the surface was nanosized due to wear. After nanocalization, more rapid diffusion channels for 'short-circuit diffusion',[38] such as grain boundaries and dislocations, were formed on the surface. These rapid diffusion channels were conducive to the diffusion of internal active elements near the surface and to the entry of external oxygen into the interior vacancies caused by the diffusion of metal atoms. Wang *et al.*[39] calculated that the diffusion coefficient between atoms in the wear-affected layer was higher (several orders of magnitude) than that in the coarse crystal. Therefore, it was reasonable to believe that the internal oxidation phenomenon was observed by EPMA.

Fig. 10 shows the HRTEM image of the wear scar section, which shows the structure and composition distribution of the passive film. It can be seen from Fig. 10a and f that the thickness of the passive film under low DOC was approximately 2 nm, which was thinner than that under high DOC. In addition, Fig. 10b–e and g–j shows the concentration distribution under different DOCs. From Fig. 10e and j, it can be seen that there was an obvious oxide layer on the surface, indicating that the area shown was the passive film of the titanium alloy. As shown by the density of EDS, the proportion of Ti, Al and V in

the region shown was significantly different from that in the matrix. The density of Al and V in this region was significantly lower than that in the matrix, and Ti was the main component of the passive film, which indicated that Ti played a dominant role in the competitive oxidation process of the passive film. Considering that the accuracy of EDS was not very good, specific component analysis still necessitated subsequent XPS analysis.

As shown in Fig. 11, the grains were mainly distributed transversely inside the wear scar. This was related to the matrix deformation caused by wear. In addition, a large number of dislocation increments and tangles were found. As shown in Fig. 11, the dislocation distribution under low DOC was larger. For better accuracy, we performed a statistical analysis on at least three HRTEM maps near the surface, and nine regions were selected from each map at the top, middle and bottom separately. The results showed that the dislocation density under high DOC (9.7×10^{16} to 11.8×10^{17} m^{-2}) was lower than that under low DOC (1.12×10^{17} to 1.22×10^{17} m^{-2}). That is, a low DOC induced an increased defect density beneath the worn surface of Ti-6Al-4V. First, wear destroyed the passive film, thus making the titanium alloy lose its protection; hence, a low DOC inhibited the process of regeneration of the passive film, thus increasing the dissolution of metal elements from the surface. Second, wear caused severe deformation of the titanium alloy near the surface within a few microns, resulting in
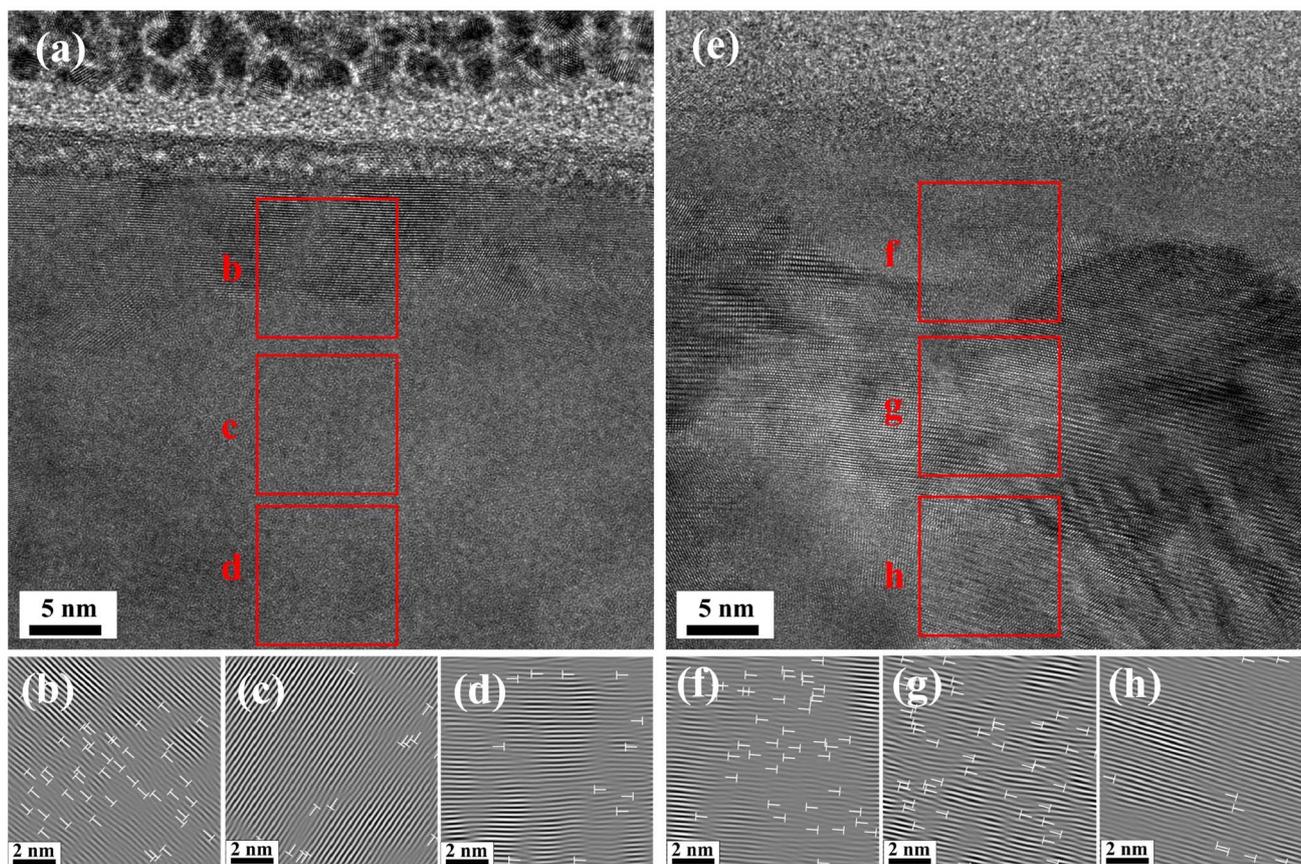

Fig. 11 HRTEM and IFFT images of the wear scar cross-section: (a–d) high DOC, (e–h) low DOC.

an increase in dislocation and providing channels for the short-circuit diffusion of metal elements. Without the protection of the passive film, metal atoms rapidly diffused through the short-circuit diffusion channels, thus leaving a larger amount of point defects in the interior of the matrix. With the accumulation and combination of point defects, an increase in the dislocation density occurred. At the same time, increasing the outward diffusion of metal atoms also accelerated the inward diffusion of oxygen atoms through these channels. Therefore, the deeper internal oxidation under low DOC observed from the EPMA results was explained.

XPS analysis

XPS was used to analyze the composition of the passive film in detail. We measured the surface outside of the wear scar (OW) and inside of the wear scar (IW), as shown in Fig. 12. The OW results reflected the effect of dissolved oxygen concentration change on the composition of the passive film, and the IW results reflected the structural difference of the regenerated passive film after the passive film was mechanically broken. For instance, as shown in Fig. 12g and j, more Ti existed in the form of oxide in the regenerated passive film, and Ti was almost nonexistent. With increasing etching depth, the original metal
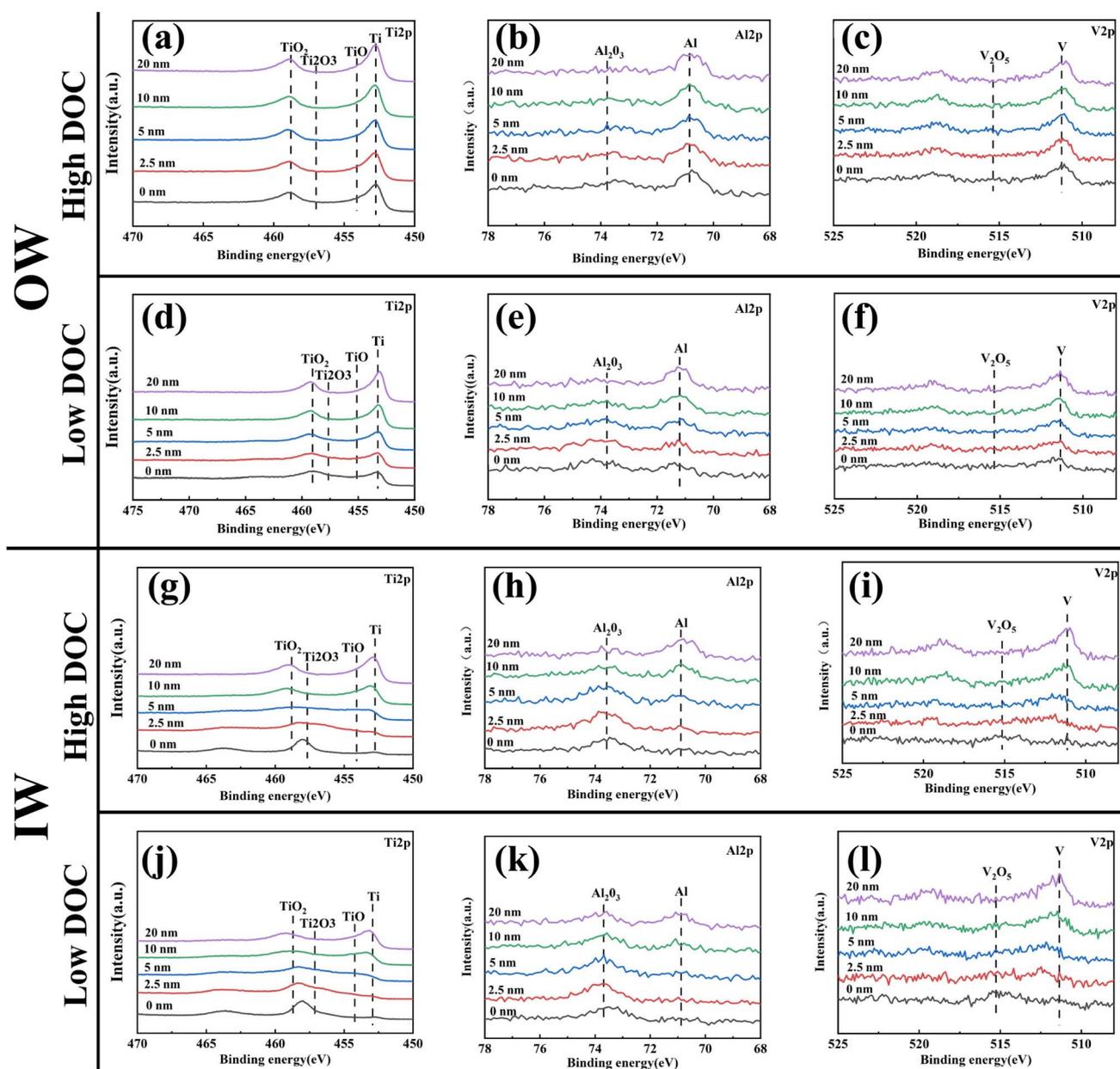

Fig. 12 XPS spectra of Ti-6Al-4V sputtered at different depths under different DOCs: (a) and (g) Ti 2p in the inside and outside of the wear scar under high DOC, (d) and (j) Ti 2p in the inside and outside of the wear scar under low DOC, (b) and (h) Al 2p in the inside and outside of the wear scar under high DOC, (e) and (k) Al 2p in the inside and outside of the wear scar under low DOC, (c) and (i) V 2p in the inside and outside of the wear scar under high DOC, (f) and (l) V 2p in the inside and outside of the wear scar under low DOC.

single substance peak was detected. From this angle, there was almost no Al at the surface (Fig. 12d and c). The peak of the Al single substance under high DOC appeared at 5 nm and that

under low DOC appeared at 10 nm, which indicated that the distribution of the Al oxide layer under low DOC was deeper (Fig. 12h and k). It can be seen from Fig. 12a, b, d and e that
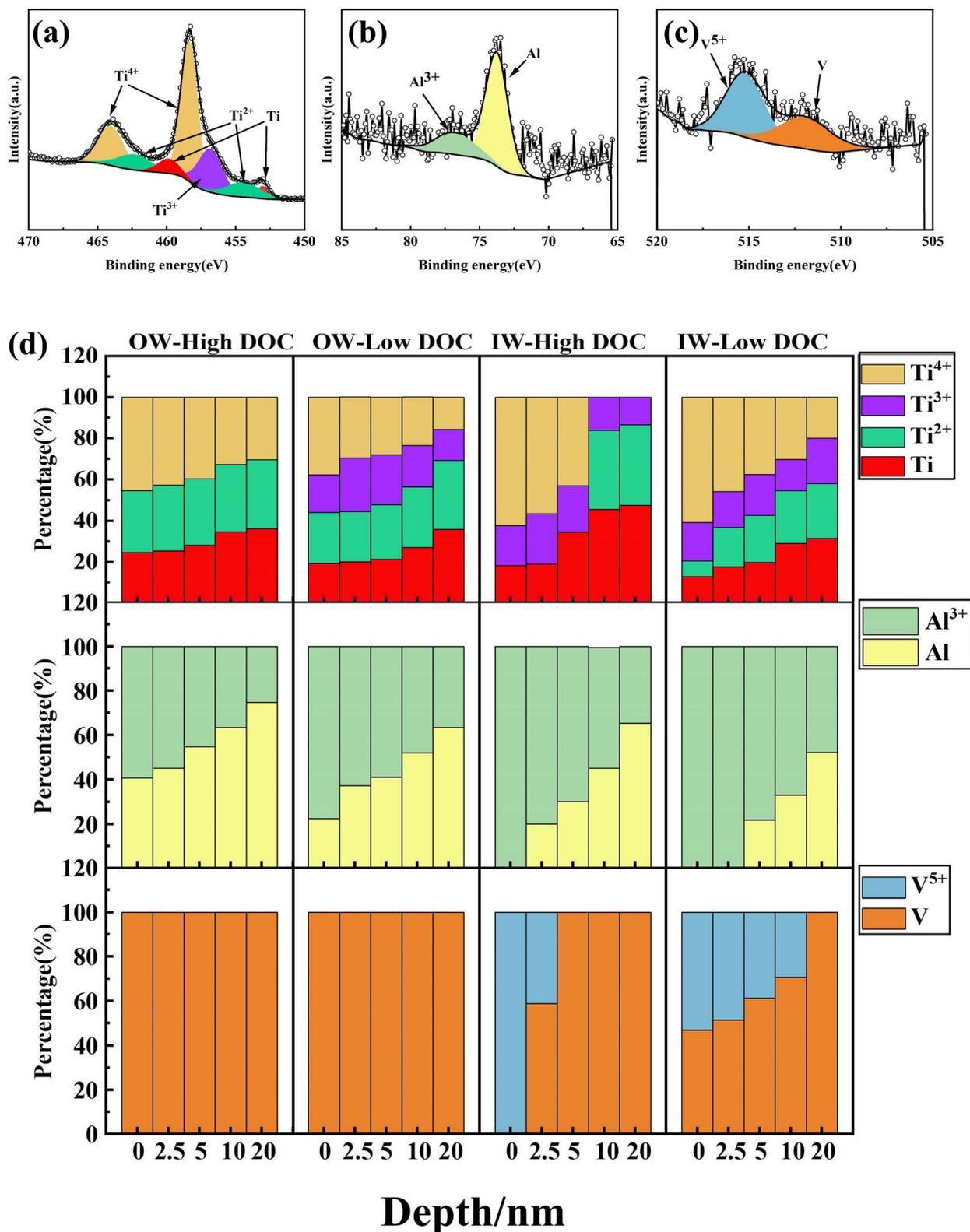

Fig. 13 (a–c) Peak fitting diagram of XPS spectrum and (d) the composition percentage of Ti, Al, V of each peak at 0, 2.5, 5, 10 and 20 nm inside and outside of the wear scar under different DOC.

Table 3 Vacancy formation energy of the Ti, Al, and V atoms in the α phase and β phase

Slab	Vacancy formation position	E_X (eV)	E_0 (eV)	μ_X (eV)	Vacancy formation energy (eV)
α(001)	Ti	−332.578	−339.993	−2.450	4.965
	Al	−336.274		−0.197	3.523
	V	−330.942		−3.573	5.478
β(110)	Ti	−338.481	−344.580	−2.450	3.649
	Al	−342.139		−0.197	2.244
	V	−337.877		−3.573	3.131

there was little Al oxide in the OW, and the peak of the Al single substance was more obvious. Compared with the Ti in the OW, Ti oxides dominated the whole surface oxides. The above phenomenon showed that when mechanical wear occurred, the passive film on the surface of the titanium alloy was doped with Al and V oxides with poor corrosion resistance. In addition, some aluminum oxide was found OW, which showed that even without mechanical wear, the lack of dissolved oxygen alone led to a decline in the protective performance of the passive film on the surface of the titanium alloy. In addition, V played no major role in this process, and only a small amount of V oxide was detected on the surface of IW.

Fig. 13 shows a schematic diagram of the metal element peaks and the proportion of different valence states of different elements at different depths. The peak fitting was carried out based on ref. [26] and [28]. As mentioned above, it was observed that the proportion of Al oxide in the outermost layer of IW reached 100%. In addition, it was observed that Ti at different depths mainly existed in four forms: Ti^{4+}, Ti^{3+}, Ti^{2+} and Ti, and the proportion of Ti^{4+} gradually decreased with increasing depth. In the IW, the proportion of higher-valence-state Ti oxides increased significantly, which indicated that the oxidation degree of the matrix after wear was higher. In the OW, the distribution of Ti oxide was deeper, and the proportion was larger under low DOC, which indicated that the decrease in dissolved oxygen concentration also led to an increase in Ti

oxides (mainly suboxide). Moreover, with increasing depth, the proportion of Al oxide decreased, and the Al single substance increased. Notably, in the IW, Al completely existed in the form of oxide in the surface layer, and the distribution of Al oxide was deeper under low DOC. This indicated that wear under low DOC promoted greater internal oxidation.

First-principles calculation

Density functional theory (DFT) was used to calculate the vacancy formation energy of three atoms in two phases.[28,40] The vacancy formation energy of different atoms was calculated, and the calculation results are shown in Table 3.

Fig. 14 shows that in the α(001) direction, the vacancy formation energies were V (5.48 eV) > Ti (4.97 eV) > Al (3.52 eV). In addition, the vacancy formation energy of β(110) was Ti (3.65 eV) > V (3.13 V) > Al (2.24 eV). The vacancy formation energy of Al in both phases was the smallest. This showed that under the same conditions, Al was more likely to separate from the matrix to form vacancies, which led to the problem of preferential dissolution. We observed that the vacancy formation energy of the metal element in the β phase was less than that in the α phase, which indicated that Ti, Al and V were more easily separated from the β phase. Metal ions were released from the matrix to form vacancies. With the increase and aggregation of vacancies, the dislocation density in the matrix increased greatly, thus accelerating the dissolution of elements.

Discussion

From the above results, it was observed that after the wear stopped under low DOC, the titanium alloy regenerated passive film was doped with a large amount of Al oxide and a small amount of V oxide, and the protective performance was greatly reduced. Fig. 15 shows a schematic diagram of the regenerated passive film after wear. First, when wear did not occur, the oxide film was not easily reduced, which was verified by XPS results. Even under low DOC, the corrosion was not aggravated because the passive film remained in the passivation state. According to the theory of phase forming film, as an independent phase, the passive film repeats the process of partial dissolution and rep-recipitation in solution.[7] When the level of dissolved oxygen decreased, the formation of Ti oxide was inhibited, so Al and V oxides participated in the formation of passive films.

Subsequently, when wear occurred, the original passive film was stripped and Ti, Al and V began to diffuse into the solution.
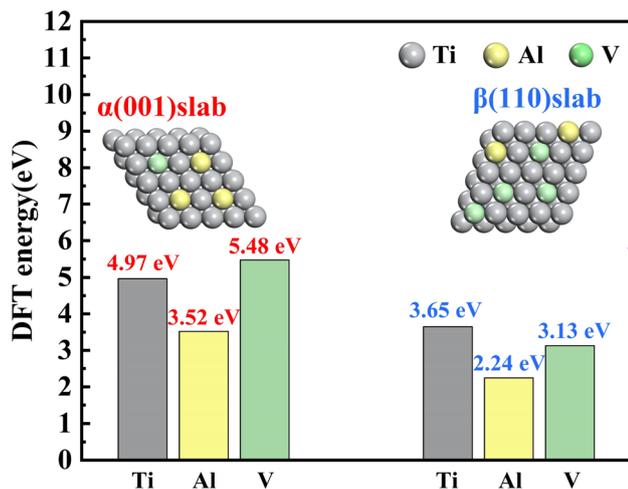

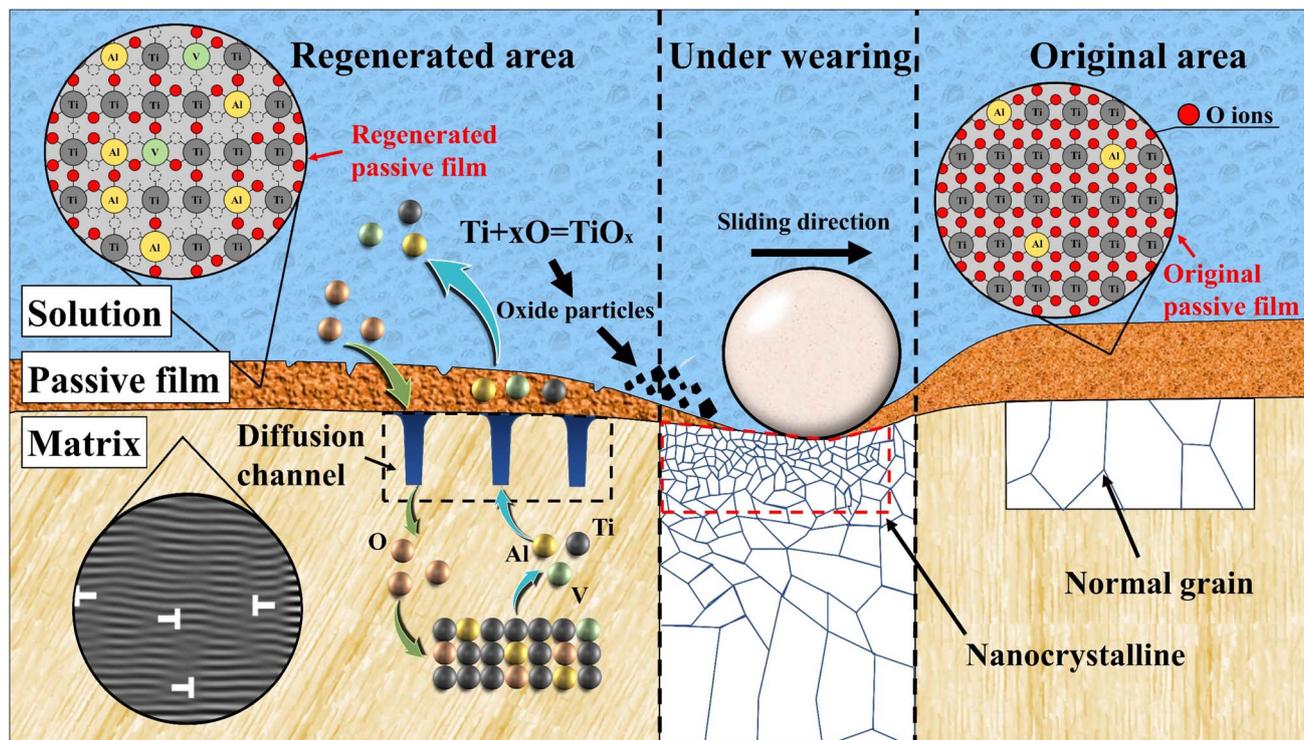**Fig. 14** Vacancy formation energies of different atoms.

Fig. 15 Schematic diagram of element dissolution and regenerated passive film during wear.

As an element with strong oxygen affinity, Ti can combine with dissolved oxygen in solution to form oxide particles and deposit on the matrix surface, which aggravated the mechanical wear loss. Hanawa *et al.*[7] found that titanium ions were very active and easily reacted with hydroxyl radicals and anions to form oxides and salts in body fluids. The point was confirmed in the XPS results (the peak value of Ti oxide at 0 nm in IW is significantly higher than that in OW). At this time, if there was not enough dissolved oxygen in the solution, the repair process of the passive film was prolonged. Due to the insufficient supply of dissolved oxygen, Ti, Al and V competed to form the passive film. Thus, a passive film doped with Al and V oxides was formed. Obviously, the passive film with a high ratio of Al and V cannot withstand the erosion of acidic solution. In addition, the erosion effect of H ions on titanium alloys was enhanced under the acidic conditions of degassing. After absorbing hydrogen, titanium forms hydrides due to its very small solution limit, which leads to embrittlement of Ti-6Al-4V and accelerates elemental dissolution.[5,41]

Moreover, the formation of internal oxidation was due to the formation of a large number of dislocations caused by wear, which provided a fast channel for the short-circuit diffusion of metal elements and formed a large number of vacancies near the surface. At the same time, oxygen also entered the metal through these short-circuit diffusion channels to form an internal oxide layer. Guleryuz *et al.* found that[42] the oxygen diffusion layer formed by the inward diffusion of oxygen becomes hard and brittle, which reduces the tensile ductility and fatigue resistance of the matrix. It indicated that a higher degree of internal oxidation may affect the life expectancy of titanium alloys under low DOC.

Conclusion

In this paper, the tribocorrosion mechanism of Ti-6Al-4V under different DOCs was studied. When titanium alloy was exposed to a relatively anoxic environment, such as that in the human body, its corrosion performance was reduced. In addition, a higher dislocation density was also produced during the wear process, leading to the preferential dissolution of elements with lower vacancy formation energy. The conclusions were drawn as follows:

(1) Electrochemical experiments showed that the corrosion performance of the passive film under low DOC was poor, and its corrosion rate was approximately 50 times higher than that under high DOC.

(2) Under low DOC, metal ions had been subjected to varying degrees of excessive dissolution. In particular, the amounts of Al and V dissolved under low DOC were 312% and 174% of those dissolved under high DOC, respectively.

(3) The original passive film was almost entirely composed of Ti oxides, while the regenerated passive film was doped with a large amount of Al and V oxides under low DOC, which greatly reduced the protective performance of the regenerated passive film.

(4) The dislocations produced by wear provided a convenient channel for element short-circuit diffusion and created a large number of vacancies in the matrix. When the sample was

exposed to air, oxygen entered the interior through these channels to induce internal oxidation.

Author contributions

Xinyu Du: conceptualization, data curation, formal analysis, methodology, writing-original draft, software. Wei Shi: resources, methodology, project administration, supervision, writing-review & editing. Song Xiang: validation, visualization. All authors read and approved the final manuscript.

Conflicts of interest

There are no conflicts to declare.

Acknowledgements

References

1 Y. Huang, J. Huang, X. Yu, S. Yu and D. Fan, Microstructure characterization and texture evolution of Ti-6Al-4V cladding layer fabricated by alterative current assisted TIG, *Surf. Coat. Technol.*, 2022, **431**, 128014.

2 B. Dutta and F. H. S. Froes, The Additive Manufacturing (AM) of titanium alloys, *Metal Powder Report*, 2017, **72**, 96–106.

3 I. Cvijović-Alagić, Z. Cvijović, S. Mitrović, V. Panić and M. Rakin, Wear and corrosion behaviour of Ti–13Nb–13Zr and Ti–6Al–4V alloys in simulated physiological solution, *Corros. Sci.*, 2011, **53**, 796–808.

4 M. Zhang, L. Xin, X. Ding, S. Zhu and F. Wang, Effects Ti/TiAlN composite multilayer coatings on corrosion resistance of titanium alloy in solid NaCl-H2O-O2 at 600°C, *J. Alloys Compd.*, 2018, **734**, 307–317.

5 T. C. Lomholt, K. Pantleon and M. A. J. Somers, In-vivo degradation mechanism of Ti-6Al-4V hip joints, *Mater. Sci. Eng., C*, 2011, **31**, 120–127.

6 W. Xu, A. Yu, X. Lu, M. Tamaddon, L. Ng, M. D. Hayat, M. Wang, *et al.*, Synergistic interactions between wear and corrosion of Ti-16Mo orthopedic alloy, *J. Mater. Res. Technol.*, 2020, **9**, 9996–10003.

7 T. Hanawa, Metal ion release from metal implants, *Mater. Sci. Eng., C*, 2004, **24**, 745–752.

8 Z. BW, H. XH and Y. GZ, Effects of dissolved oxygen on the electrochemical corrosion behavior of pure titanium in fluoride-containing weakly acidic solutions, *J. Solid State Electrochem.*, 2018, **22**, 2083–2093.

9 Z. BW, H. XH and Y. GZ, Evaluation of the dissolved oxygen-related electrochemical behavior of pure titanium in acidic fluoride-containing solutions, *J. Solid State Electrochem.*, 2016, **20**, 3549–3571.

10 X. Li, X. Meng, Q. Zhang, H. Cai, Z. Yan, L. Wu and F. Cao, In Situ Studies of Hydrogen Evolution Kinetics on Pure Titanium Surface: The Effects of Pre-Reduction and Dissolved Oxygen, *J. Phys. Chem. C*, 2022, **126**, 1828–1844.

11 J. Guan, X. Jiang, Q. Xiang, F. Yang and J. Liu, Corrosion and tribocorrosion behavior of titanium surfaces designed by electromagnetic induction nitriding for biomedical applications, *Surf. Coat. Technol.*, 2021, **409**, 126844.

12 D. C. T. Juliana, B. Claudemiro and C. D. R. Andréa, Comparative analysis of corrosion resistance between beta titanium and Ti-6Al-4V alloys: A systematic review, *J. Trace Elem. Med. Biol.*, 2020, **62**, 126618.

13 J. Li, Y. He, W. Shi, S. Xiang and W. Gao, Different passivation behavior between α and β phases of Ti-6Al-4V in HCl solutions under oxygenated/deoxygenated conditions, *Appl. Surf. Sci.*, 2022, **604**, 154539.

14 J. Grabarczyk, J. Gaj, B. Pazik, W. Kaczorowski and B. Januszewicz, Tribocorrosion behavior of Ti6Al4V alloy after thermo-chemical treatment and DLC deposition for biomedical applications, *Tribol. Int.*, 2021, **153**, 106560.

15 P. Stenlund, O. Omar, U. Brohede, S. Norgren, B. Norlindh, A. Johansson, J. Lausmaa, *et al.*, Bone response to a novel Ti–Ta–Nb–Zr alloy, *Acta Biomater.*, 2015, **20**, 165–175.

16 D. F. Ferreira, S. M. A. Almeida, R. B. Soares, L. Juliani, A. Q. Bracarense, V. D. F. C. Lins and R. M. R. Junqueira, Synergism between mechanical wear and corrosion on tribocorrosion of a titanium alloy in a Ringer solution, *J. Mater. Res. Technol.*, 2019, **8**, 1593–1600.

17 I. Hacisalihoglu, A. Samancioglu, F. Yildiz, G. Purcek and A. Alsaran, Tribocorrosion properties of different type titanium alloys in simulated body fluid, *Wear*, 2015, **332–333**, 679–686.

18 A. Revathi, S. Magesh, K. B. Vamsi, D. Mitun and M. Geetha, Current advances in enhancement of wear and corrosion resistance of titanium alloys – a review, *Mater. Technol.*, 2016, **31**, 696–704.

19 A. Manoj, A. K. Kasar and P. L. Menezes, Tribocorrosion of Porous Titanium Used in Biomedical Applications, *J. Bio-Tribo-Corros.*, 2019, **5**, 3.

20 W. Kheder, S. Al Kawas, K. Khalaf and A. R. Samsudin, Impact of tribocorrosion and titanium particles release on dental implant complications — A narrative review, *Jpn Dent. Sci. Rev.*, 2021, **57**, 182–189.

21 V. Dalbert, N. Mary, B. Normand, C. Verdu and S. Saedlou, In situ determinations of the wear surfaces, volumes and kinetics of repassivation: Contribution in the understanding of the tribocorrosion behaviour of a ferritic stainless steel in various pH, *Tribol. Int.*, 2020, **150**, 106374.

22 V. Gopal and G. Manivasagam, Wear – Corrosion synergistic effect on Ti–6Al–4V alloy in H2O2 and albumin environment, *J. Alloys Compd.*, 2020, **830**, 154539.

23 P. A. Vendittoli, C. Riviere, A. G. Roy, J. Barry, D. Lusignan and M. Lavigne, Metal-on-metal hip resurfacing compared with 28-mm diameter metal-on-metal total hip replacement: a randomised study with six to nine years' follow-up, *J. Bone Joint Surg.*, 2013, **95**, 1464–1473.

24 X. Lu, D. Zhang, W. Xu, A. Yu, J. Zhang, M. Tamaddon, J. Zhang, *et al.*, The effect of Cu content on corrosion, wear and tribocorrosion resistance of Ti-Mo-Cu alloy for load-bearing bone implants, *Corros. Sci.*, 2020, **177**, 109007.

25 M. K. Dimah, F. Devesa Albeza, V. Amigó Borrás and A. Igual Muñoz, Study of the biotribocorrosion behaviour of titanium biomedical alloys in simulated body fluids by electrochemical techniques, *Wear*, 2012, **294–295**, 409–418.

26 X. Li, L. Wang, L. Fan, Z. Cui and M. Sun, Effect of temperature and dissolved oxygen on the passivation behavior of Ti–6Al–3Nb–2Zr–1Mo alloy in artificial seawater, *J. Mater. Res. Technol.*, 2022, **17**, 374–391.

27 G. Kresse and J. Furthmuller, Efficient iterative schemes for ab initio total-energy calculations using a plane-wave basis set, *Phys. Rev. B: Condens. Matter Mater. Phys.*, 1996, **54**, 11169–11186.

28 J. Li, Y. He, W. Shi, S. Xiang and W. Gao, Different passivation behavior between α and β phases of Ti-6Al-4V in HCl solutions under oxygenated/deoxygenated conditions, *Appl. Surf. Sci.*, 2022, **604**, 154539.

29 Y. Cheng, L. Zhu, G. Wang, J. Zhou, S. R. Elliott and Z. Sun, Vacancy formation energy and its connection with bonding environment in solid: A high-throughput calculation and machine learning study, *Comput. Mater. Sci.*, 2020, **183**, 109803.

30 D. G. Li, J. D. Wang, D. R. Chen and P. Liang, Influence of passive potential on the electronic property of the passive film formed on Ti in 0.1M HCl solution during ultrasonic cavitation, *Ultrason. Sonochem.*, 2016, **29**, 48–54.

31 T. Shibata and Y. C. Zhu, The effect of film formation conditions on the structure and composition of anodic oxide films on titanium, *Corros. Sci.*, 1995, **37**, 253–270.

32 L. Wang, H. Yu, S. Wang, L. Qiao and D. Sun, In-situ XAFS and SERS study of self-healing of passive film on Ti in Hank's physiological solution, *Appl. Surf. Sci.*, 2019, **496**, 143657.

33 I. H. Elshamy, S. S. Abd El Rehim, M. A. M. Ibrahim and N. F. El Boraei, The bifunctional role played by thiocyanate anions on the active dissolution and the passive film of titanium in hydrochloric acid, *Corros. Eng., Sci. Technol.*, 2022, **57**, 542–552.

34 A. Iwabuchi, J. W. Lee and M. Uchidate, Synergistic effect of fretting wear and sliding wear of Co-alloy and Ti-alloy in Hanks' solution, *Wear*, 2007, **263**, 492–500.

35 M. K. Dimah, F. Devesa Albeza, V. Amigó Borrás and A. Igual Muñoz, Study of the biotribocorrosion behaviour of titanium biomedical alloys in simulated body fluids by electrochemical techniques, *Wear*, 2012, **294–295**, 409–418.

36 M. Metikoš-Huković, A. Kwokal and J. Piljac, The influence of niobium and vanadium on passivity of titanium-based implants in physiological solution, *Biomaterials*, 2003, **24**, 3765–3775.

37 E. Sharifikolouei, B. Sarac, A. Micoulet, R. Mager, M. Watari-Alvarez, E. Hadjixenophontos, Z. Burghard, *et al.*, Improvement of hardness in Ti-stabilized austenitic stainless steel, *Mater. Des.*, 2022, **223**, 111242.

38 B. J. Hansen, H. I. Chan, J. Lu, G. Lu and J. Chen, Short-circuit diffusion growth of long bi-crystal CuO nanowires, *Chem. Phys. Lett.*, 2011, **504**, 41–45.

39 X. Wang, D. Mao, X. Wei and W. Wang, Cr atom diffusion in tribolayer T10 steel induced by dry sliding against 20CrMnTi steel, *Appl. Surf. Sci.*, 2013, **270**, 145–149.

40 Y. Zhu, W. Zheng, Y. Pan, Y. Pan, T. Liu, X. Zhou, D. Shi, *et al.*, Formation and binding energies of vacancies in the Al(111) surface: Density functional theory calculations confirm simple bond model, *Surf. Sci.*, 2015, **637–638**, 85–89.

41 F. Huang, Y. Zhu, M. Yu, L. Wen and Y. Jin, Synergistic Effects of Hydrostatic Pressure and Dissolved Oxygen on the SCC Behavior of Hydrogenated Ti6Al4V Alloy in Deep-Sea Environment, *Metals*, 2023, **13**, 449.

42 H. Guleryuz and H. Cimenoglu, Oxidation of Ti–6Al–4V alloy, *J. Alloys Compd.*, 2009, **472**, 241–246.